NASA TECHNICAL MEMORANDUM

NASA TM X-2485

NASA TM X-2485

DESIGN AND PERFORMANCE OF AN 0.8-HUB-TIP-RATIO AXIAL-FLOW PUMP ROTOR WITH A BLADE-TIP DIFFUSION FACTOR OF 0.55

by Donald C. Urasek

Lewis Research Center

Cleveland, Ohio 44135

NATIONAL AERONAUTICS AND SPACE ADMINISTRATION • WASHINGTON, D. C. • JANUARY 1972

1. Report No.	2. Government Accession No.	3. Recipient's Catalog No.
NASA TM X-2485		

4. Title and Subtitle	5. Report Date
DESIGN AND PERFORMANCE OF AN 0.8-HUB-TIP-RATIO AXIAL-FLOW PUMP ROTOR WITH A BLADE-TIP DIFFUSION FACTOR OF 0.55	January 1972
	6. Performing Organization Code

7. Author(s)	8. Performing Organization Report No.
Donald C. Urasek	E-6423
	10. Work Unit No. 764-74

9. Performing Organization Name and Address	11. Contract or Grant No.
Lewis Research Center National Aeronautics and Space Administration Cleveland, Ohio 44135	
	13. Type of Report and Period Covered Technical Memorandum
12. Sponsoring Agency Name and Address National Aeronautics and Space Administration Washington, D.C. 20546	14. Sponsoring Agency Code

15. Supplementary Notes

16. Abstract

A 22.9-centimeter (9-in.) diameter axial-flow rotor with a 0.8 hub-tip radius ratio, a design flow coefficient of 0.466, and a blade tip design diffusion factor of 0.55 was tested in cold water under both cavitating and noncavitating conditions. Radial surveys of the flow conditions at the rotor inlet and outlet were made. At design flow, the rotor produced an overall headrise coefficient of 0.360 with an overall efficiency of 95.0 percent. The efficiency remained greater than 88 percent over the entire flow coefficient range which varied from 0.350 to 0.615.

17. Key Words (Suggested by Author(s))	18. Distribution Statement
Axial-flow pump performance Water Blade-element performance	Unclassified - unlimited

19. Security Classif. (of this report)	20. Security Classif. (of this page)	21. No. of Pages	22. Price*
Unclassified	Unclassified	27	$3.00

* For sale by the National Technical Information Service, Springfield, Virginia 22151

DESIGN AND PERFORMANCE OF AN 0.8-HUB-TIP-RATIO AXIAL-FLOW PUMP ROTOR WITH A BLADE-TIP DIFFUSION FACTOR OF 0.55

by Donald C. Urasek

Lewis Research Center

SUMMARY

A 22.9-centimeter (9-in.) diameter axial-flow rotor with a 0.8 hub-tip radius ratio, a design flow coefficient of 0.466, and a blade-tip design diffusion factor of 0.55 was tested. The tests were conducted in 300 K (80° F) water under both cavitating and noncavitating flow conditions. Detailed radial surveys of the flow conditions at the rotor inlet and outlet were made, and flow and performance parameters were calculated across a number of selected blade elements. The stall hysteresis was recorded at three blade-element locations, and definitions of the outer casing boundary layer were obtained at the rotor inlet and outlet measuring stations.

Radial surveys at the rotor outlet indicated that three-dimensional flows affected both the outlet flow coefficient and deviation angle distributions in the rotor tip region. At design flow the rotor produced an overall headrise coefficient of 0.360, as compared with a design value of 0.365. An overall hydraulic efficiency of 95.0 percent was achieved experimentally as compared with a design value of 92.9 percent. The efficiency remained greater than 88 percent over the entire flow coefficient range, which varied from 0.350 to 0.615.

INTRODUCTION

A study was conducted at the Lewis Research Center to determine the effects of blade loading on the performance characteristics of axial-flow rotors. The study has provided a better understanding of the flow characteristics over a range of operating conditions, an evaluation of performance limitations, and an experimental evaluation of design techniques. The measure of blade loading in this study is the D-factor (diffusion factor) developed in reference 1. Values of this parameter varied from D = 0.26 to 0.66. The design and performance results of these rotors are discussed in references 2

to 5. These rotor blades have double-circular-arc airfoil sections with relatively short chords and have high hub-tip radius ratios. These high hub-tip ratio axial-flow rotors are typically used as latter stages of multistage pumps or where good cavitation performance is not required.

The design radial distributions of deviation angle and flow losses for the rotors used in this study were based essentially on two-dimensional flow. Results indicated that this simplified design system was adequate to predict the radial distributions of deviation angle and flow losses for the rotors with blade tip D-factors of 0.25 and 0.43 as reported in references 2 and 3, respectively. The rotors reported in references 4 and 5 were considered to be highly loaded, having been designed with blade tip D-factors of 0.63 and 0.66, respectively. Radial survey trends of deviation angle and flow losses indicated that strong three-dimensional flow effects were present at the rotor outlet. The two-dimensional design system would have to be modified to account for these three-dimensional effects as discussed in reference 5.

The results of the reference studies indicate a substantial increase in three-dimensional flow effects as the loading level at the blade tip increased from a D-factor of 0.43 to 0.63. This investigation was conducted specifically to determine the trends in three-dimensional effects at a loading level intermediate to those of the previous studies. The rotor tip D-factor was 0.55.

In the investigation reported herein, the performance of 22.9-centimeter (9-in.) diameter axial-flow pump rotor having a hub-tip ratio of 0.8 and a blade tip D-factor of 0.55 is evaluated. The rotor tests were conducted 300 K (80° F) water at a rotative speed of 3000 rpm. This report presents the blade design, the measured overall performance, and variations of flow conditions and performance of a selected number of blade elements over a range of noncavitating operating conditions. As flow was reduced into the blade stall region, the stall hysteresis patterns were measured and are shown at three radial blade element locations. Limited data taken at reduced inlet pressure are shown to indicate the level of inlet pressure required for this stage to operate with no loss in performance. Measurements were made to define the outer-wall boundary layer at the blade inlet and outlet measuring stations.

ROTOR DESIGN

The design for this rotor used a blade-element flow theory. The velocity diagrams were calculated at the rotor inlet and outlet, and double-circular-arc blade-section profiles were designed on a number of cylindrical surfaces of revolution. The blade elements were stacked on a radial line through the center of gravity of the individual sections.

The selected design values for this rotor are

Flow coefficient, φ	0.466
D-factor at tip	0.55
Hub-tip radius ratio	0.80
Tip diameter, cm (in.)	22.9 (9)

The blade-element design procedure is described in detail in reference 6. The velocity diagram design values computed for this rotor are shown in table I. The values are based on no inlet prewhirl. The blade design values are listed in table II. A photograph of the rotor is shown in figure 1.

TABLE I. - VELOCITY DIAGRAM DESIGN VALUES

[$V_{\theta,1} = 0$; $U_{T,1} = U_{T,2} = 118$ ft/sec (36 m/sec).]

Radius ratio, r/r_t	Outlet flow coefficient, φ	Relative inlet flow angle, β_1', deg	Change in relative flow angle, $\Delta\beta'$, deg	Rotor head-rise coefficient, ψ	Blade diffusion factor, D	Total head-loss coefficient, $\overline{\omega}$
1.00	0.425	65.0	11.2	0.350	0.556	0.115
.95	.448	63.9	13.9	.357	.526	.069
.90	.472	62.6	17.8	.365	.536	.044
.85	.491	61.3	22.2	.373	.536	.024
.80	.488	59.8	26.5	.371	.555	.027

TABLE II. - BLADE DESIGN VALUES

[Number of blades, 19; chord length, 1.51 in. (3.84 cm) blade tip diameter, 9 in. (22.8 cm).]

Radius ratio, r/r_t	Incidence angle, i, deg	Deviation angle, δ deg	Camber angle, φ^o, deg	Solidity, σ	Setting angle, γ deg	Ratio of maximum thickness to chord T_{max}/C
0.98	-3.0	10.2	25.2	1.02	54.9	0.071
.94	-2.3	9.6	26.4	1.06	52.7	.075
.90	-1.7	9.5	29.0	1.11	49.8	.079
.86	-1.2	9.2	31.7	1.16	46.9	.083
.82	-.3	8.8	33.9	1.22	43.7	.087

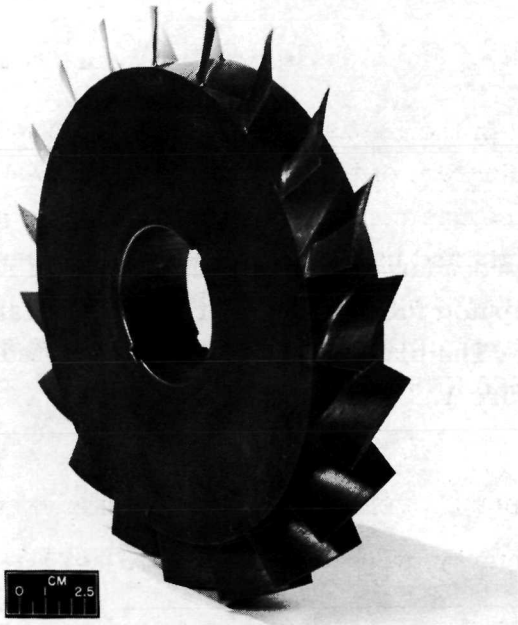

C-69-3581

Figure 1. - Axial-flow rotor.

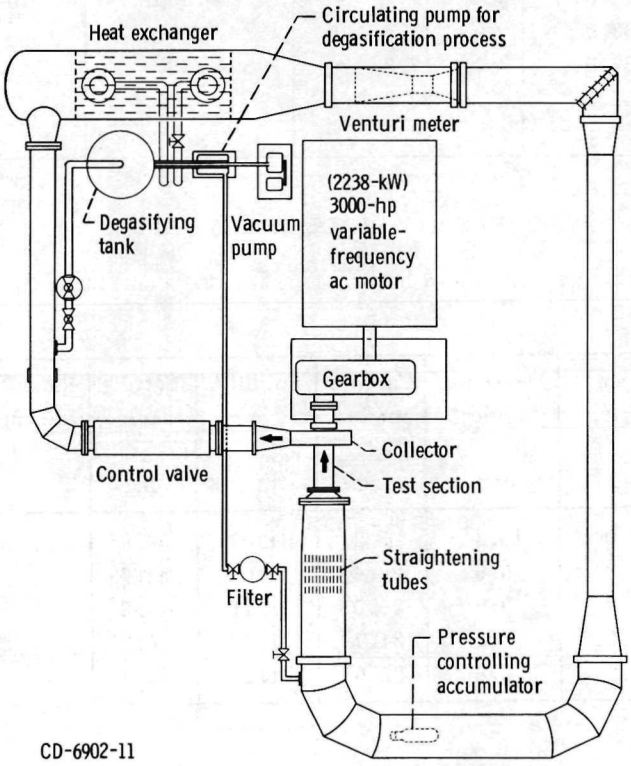

Figure 2. - Lewis water tunnel.

APPARATUS AND PROCEDURE

Test Facility

The rotor was tested in the Lewis water tunnel which is described in detail in reference 2. A schematic diagram of the test facility is shown in figure 2. Before the tests, the water in the loop was conditioned by reducing the gas content to approximately 1 part per million by weight and by circulating the water through a filter capable of removing solid particles larger than 5 micrometers. During tests, the gas content was maintained below 3 parts per million by weight, and the water temperature was maintained at approximately 300 K (80° F).

Instrumentation

Photographs of the survey probes are shown in figure 3. Total pressure and flow

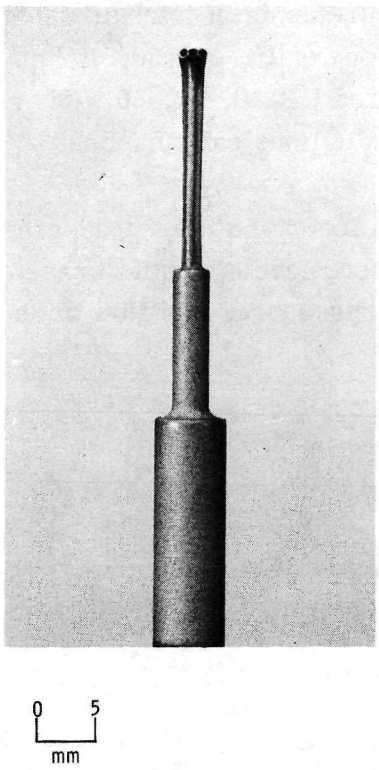

(a) Cobra probe.

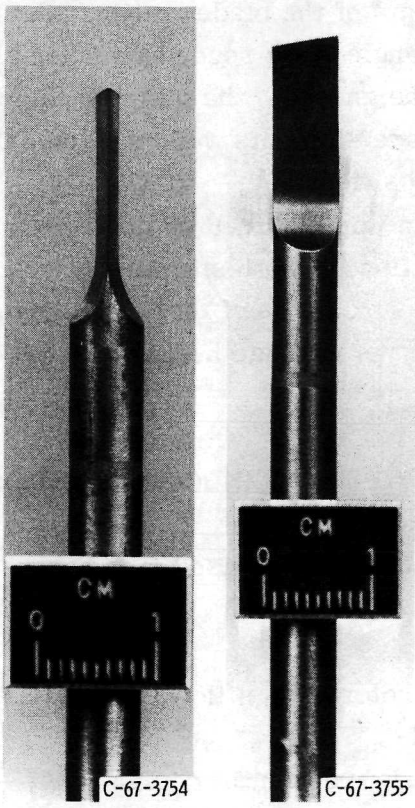

Front view Side view

(b) Static-pressure wedge.

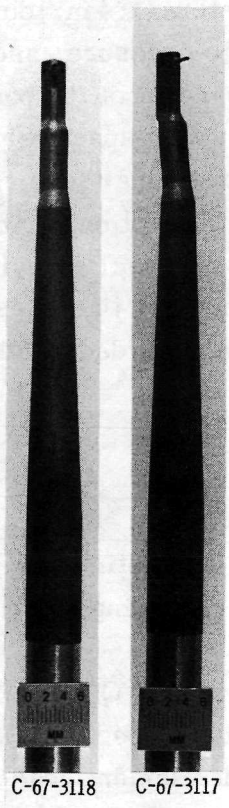

Front view Side view

(c) Boundary-layer probe measuring angle and total pressure.

Figure 3. Probes.

angle were measured with the cobra probe (fig. 3(a)), and static pressure was measured with the wedge probe (fig. 3(b)). Each probe had associated null-balancing, stream-direction-sensitive equipment that automatically alined the probe to the direction of flow. Each wedge static probe was calibrated in a low-speed air tunnel. The distribution of total pressure and flow angle across the boundary layer on the outer wall was measured with the probe shown in figure 3(c). Additional instruments included a venturi flowmeter to measure flow rate and an electronic speed counter used in conjunction with a magnetic pickup to measure rotor rpm.

Test Procedure

The noncavitating performance characteristics were obtained by maintaining the inlet pressure and rotative speed constant while varying the flow. At each selected flow the radial distributions of flow conditions were surveyed at measuring stations located approximately 2.54 centimeters (1 in.) upstream of the blade leading edge and 3.5 centimeters (1.4 in.) downstream of the blade trailing edge. Measurements of total pressure, static pressure, and flow angle were recorded at radial positions of 10, 30, 50, 70 and 90 percent of the passage height from the outer walls (designated RP-10, 30, 50, 70, and 90, respectively). Blade elements were assumed to lie on cylindrical surfaces intersecting these radial positions.

Cavitation performance was obtained by holding rotational speed and inlet pressure constant while varying the flow. The tests were conducted at four levels of inlet pressure. For these tests measurements of total pressure, static pressure, and flow angle were recorded at 50 percent of passage height (RP-50) only.

Data Accuracy and Reliability

The estimated errors of the data based on inherent accuracies of the instrumentation and recording systems are as follows:

Flow rate, Q_V, percent of rotor design flow	±1.0
Rotative speed, N, percent	±0.5
Blade element head rise, ΔH, percent at design flow	±1.0
Velocity head, $V^2/2g$, percent at design flow	±1.5
Flow angle, β, deg	±1.0
Net positive suction head, NPSH, m (ft)	±0.3 (±1.0)

The symbols are defined in appendix A. The equations for calculating the selected blade element and overall performance parameters are presented in appendix B.

The primary method for determining the reliability of the measured data is through comparisons of the integrated weight flows at the blade inlet and outlet measuring stations with the values measured with the venturi meter. These comparisons are presented in figure 4. The difference between the integrated and the venturi-measured flows at the inlet measuring station were approximately 4 percent of the venturi flow over the whole flow range of the test rotor. The integrated flows at the outlet measuring station differ from the venturi-measured flow somewhat more than usual, being about 8 percent less at flow coefficients of 0.42 and below.

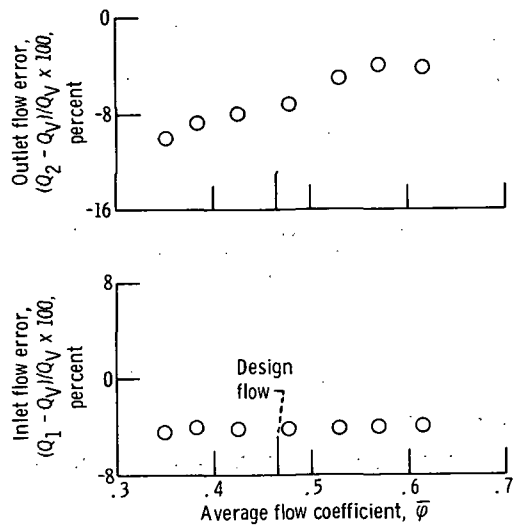

Figure 4. - Comparison of integrated flows at blade inlet and outlet with those measured by venturi meter.

RESULTS AND DISCUSSION

Overall Performance

Noncavitating performance. - The noncavitating overall performance curves for the pump rotor are shown in figure 5 where mass averaged head-rise coefficient $\overline{\psi}$ and mass averaged efficiency $\overline{\eta}$ are plotted as functions of average flow coefficient $\bar{\varphi}$. The average flow coefficient is based on venturi measured flow, inlet geometric area, and blade-tip speed as defined in appendix B. The characteristic curve was limited at low flows by unstable flow conditions evidenced by rig vibrations and noise (stalled condition) and at high flows by the pressure-loss characteristic of the test loop.

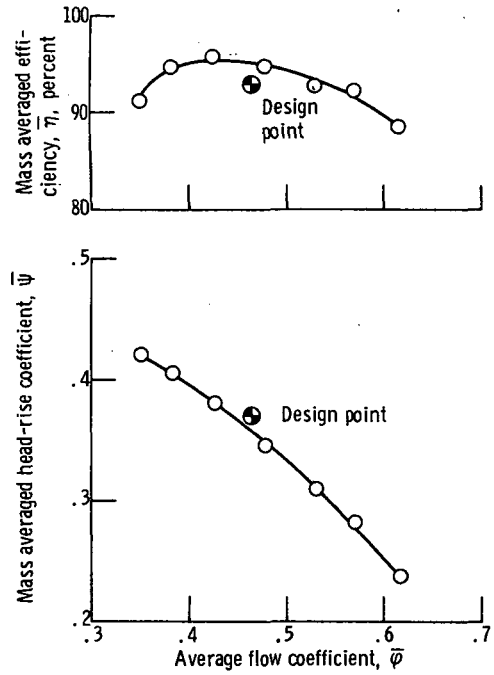

Figure 5. - Overall performance of axial-flow pump rotor (noncavitating). Rotor tip speed, 36 meters per second (118 ft/sec); net positive suction head, 130 meters (425 ft).

From the casing boundary-layer measurements (see appendix C) a flow blockage factor of 1.29 percent was determined for design flow at the rotor inlet. Therefore, the design inlet flow diagrams should be achieved at a measured average flow coefficient of

$$\bar{\varphi} = (1.0 - 0.0129)\,\bar{\varphi}_{des}$$

$$\bar{\varphi} = (0.9871)(0.466) = 0.460$$

The inlet flow coefficient of 0.460 is used as the value for comparison of measured and design parameters. At $\bar{\varphi} = 0.460$ the mass averaged headrise coefficient of 0.360 is slightly below the design value of 0.365. Design efficiency was 92.9 percent; an overall hydraulic efficiency of 95.0 percent was achieved experimentally. The data showed that the efficiency remained high (greater than 88 percent) over the entire flow coefficient range which varied from $\bar{\varphi} = 0.350$ to 0.615.

Cavitating performance. - A limited amount of cavitation data were obtained for this rotor to determine the net positive suction head (NPSH) requirements using midspan instrumentation only. A cavitating characteristic performance curve is presented in figure 6 where rotor head-rise coefficient ψ measured at midspan (RP-50) is plotted

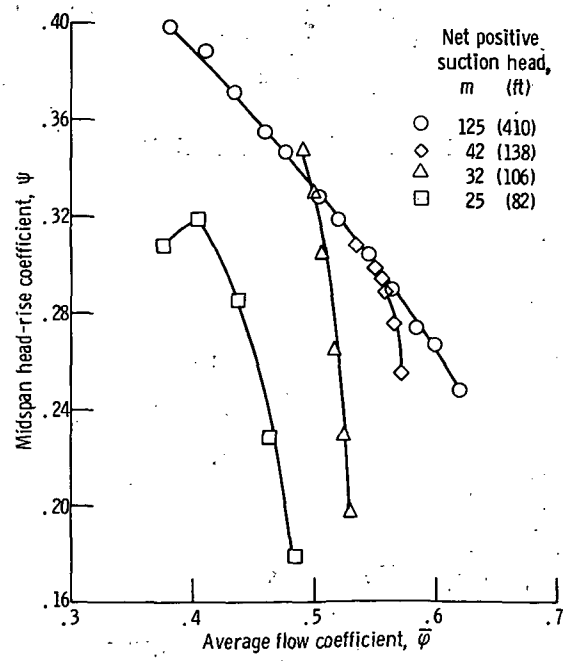

Figure 6. - Midspan performance curves of axial-flow pump rotor (cavitating). Rotor tip speed, 36 meters per second (118 ft/sec).

over the range of flows for four values of NPSH. A curve of noncavitating midspan head rise at an NPSH value of 125 meters (410 ft) is plotted to provide a basis for comparison. The blade-element data presented in the following section were all taken with a pressure at the rotor inlet sufficient to supress cavitation (NPSH value of 125 m (410 ft).

Blade Element Performance

Radial distributions. - The radial distributions of flow and selected blade-element performance parameters for three flow coefficients are presented in figure 7. Radial distribution plots permit a detailed examination of blade performance and indicate the range of flow conditions a succeeding stator row would be required to accept.

The radial distribution of parameters at the rotor outlet indicate departure from the two-dimensional flow assumed in the design. Two parameters reflecting three-dimensional flow effects are the outlet flow coefficient and deviation angle. When compared with design, both the outlet flow coefficient and deviation angle showed significant differences in both level and distribution in the tip region. The two highly loaded rotors, which experienced three-dimensional flow effects (refs. 4 and 5), showed similar dif-

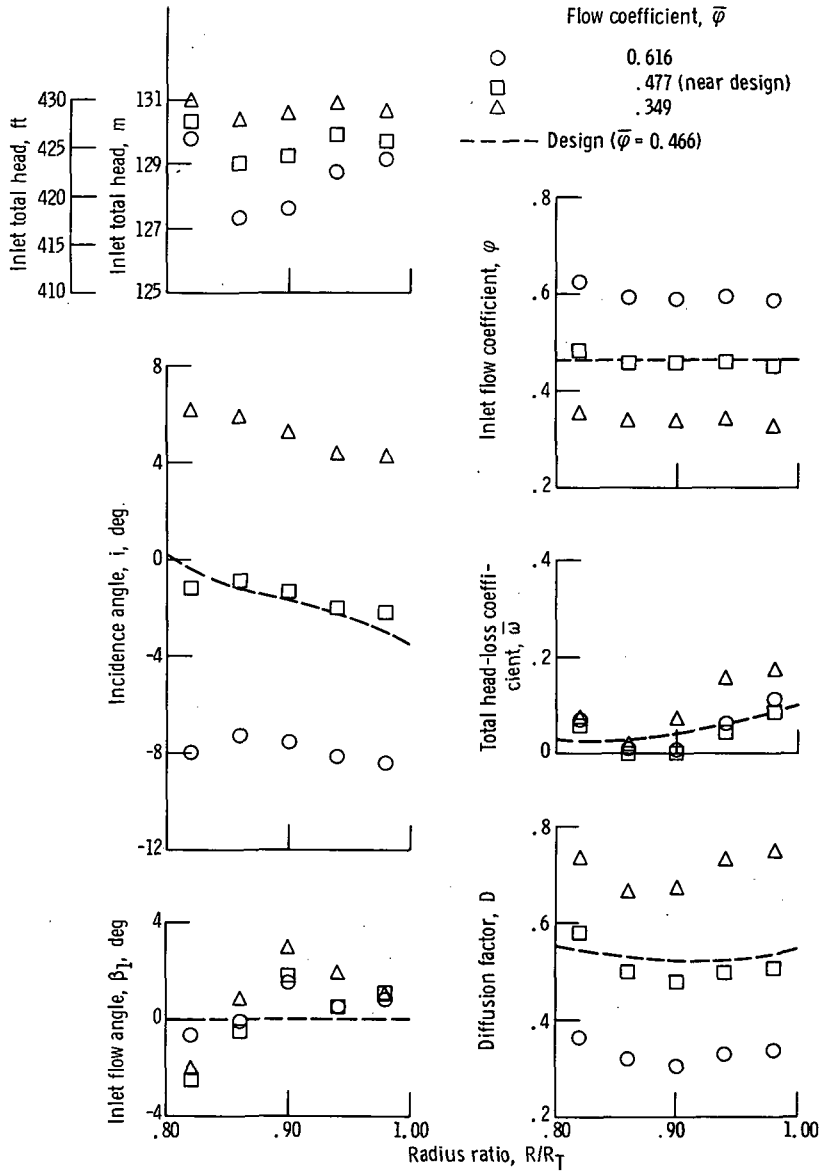

Figure 7. - Radial distributions of blade-element flow and performance parameters (noncavitating). Rotor tip speed, 36 meters per second (118 ft/sec); net positive suction head, 130 meters (425 ft).

ferences in both level and distribution of outlet flow coefficient and deviation angle. However, the differences in deviation angle from design values were greater and extended over a greater portion of the blade height for the highly loaded rotors. The outlet flow coefficient distribution in the tip region was significantly lower than design, which is apparently caused by a radial shifting of the flow toward midpassage. This is substantiated by slightly higher than design values of flow coefficient near midpassage.

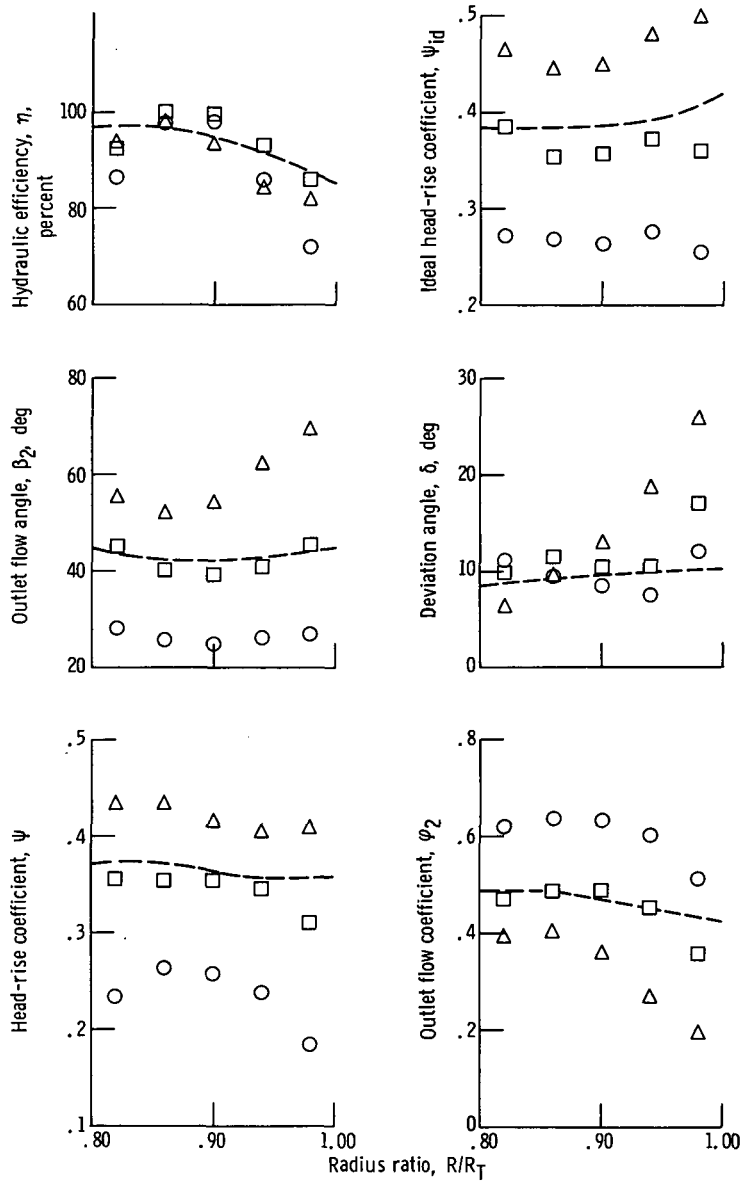

Figure 7. - Concluded.

Variations with incidence angle. - The variations of selected blade-element performance parameters with incidence angle are presented in figure 8 for five blade elements designated as RP-10, 30, 50, 70, and 90.

The incidence angles at which minimum losses occurred are defined at all five radial measuring stations. For each of the elements, the minimum loss incidence angles quite closely with the design values presented in table II. The loss coefficient $\overline{\omega}$ increased at all five radial measuring stations as the rotor approached stall (increasing

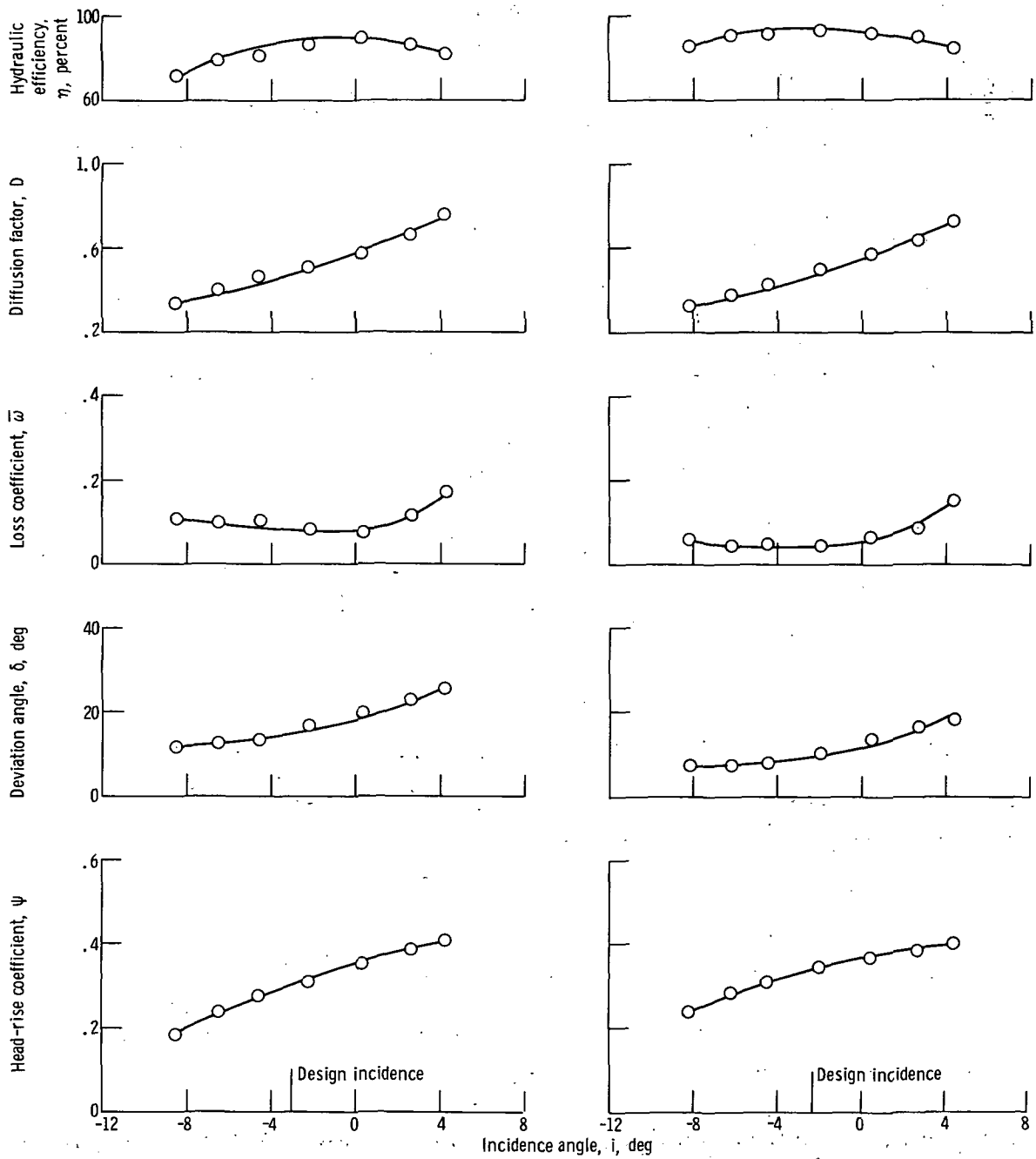

(a) Blade element located at 10 percent of passage height from tip. Radius ratio, 0.98 (RP-10).

(b) Blade height located at 30 percent of passage height from tip. Radius ratio, 0.94 (RP-30).

Figure 8. - Rotor blade-element performance characteristics (noncavitating). Rotor tip speed, 36 meters per second (118 ft/sec); net positive suction head, 130 meters (425 ft).

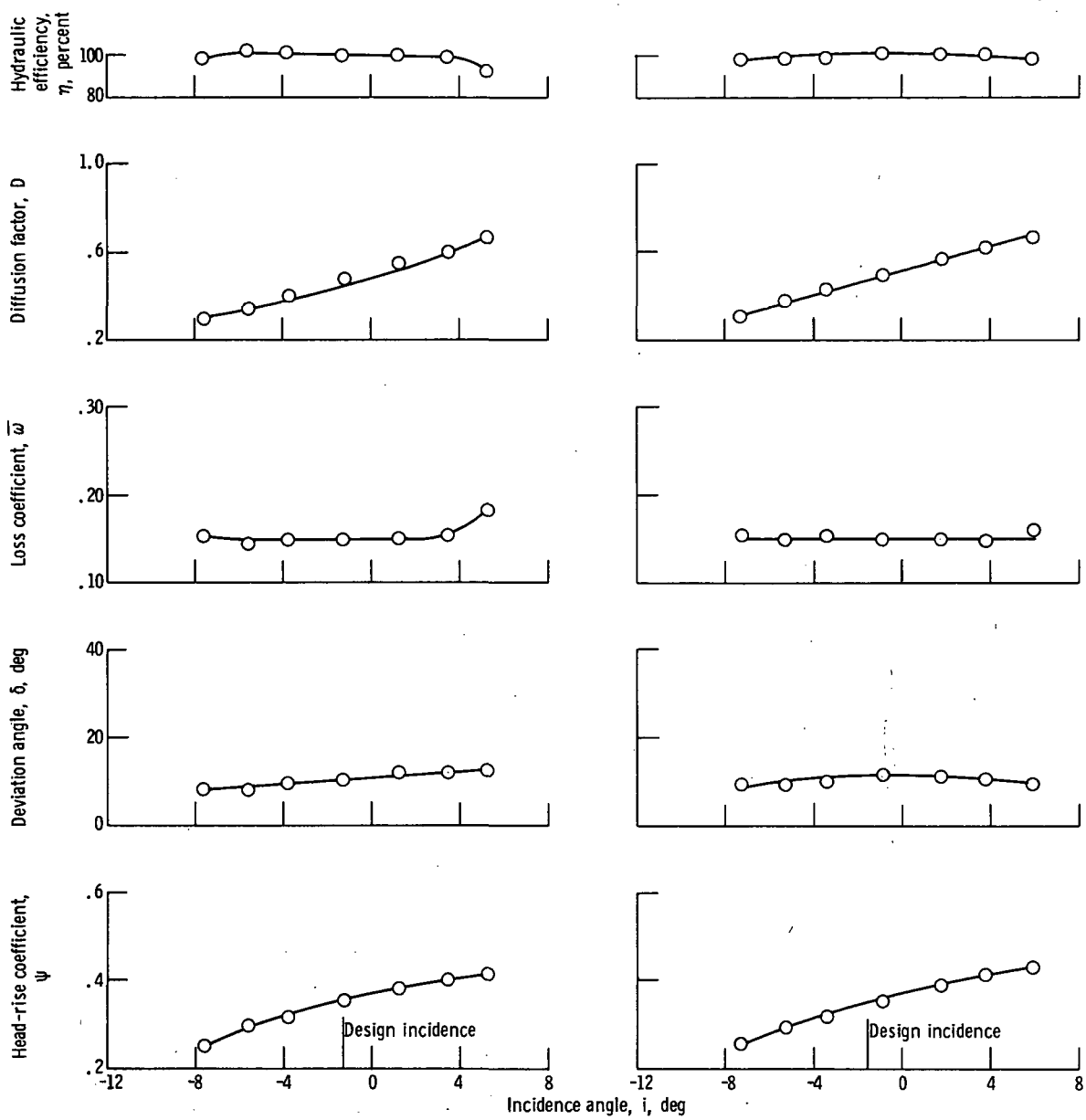

(c) Blade element located at 50 percent of passage height from tip. Radius ratio, 0.90 (RP-50).

(d) Blade element located at 70 percent of passage height from tip. Radius ratio, 0.86 (RP-70).

Figure 8. - Continued.

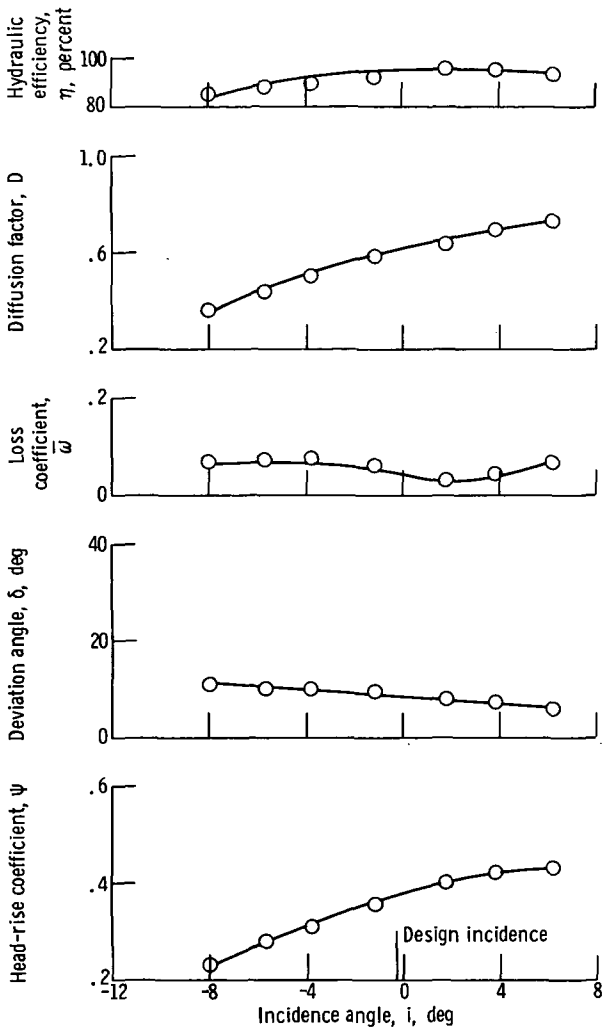

(e) Blade element located at 90 percent of passage height from tip. Radius ratio, 0.82 (RP-90).

Figure 8. - Concluded.

incidence angle). The loss coefficient at the RP-10 and RP-30 locations increased at a much greater rate than at the other three blade-element locations as the rotor approached stall, which indicates that the tip portion of the rotor blade would probably stall first. Stall occurred at an incidence angle of approximately 4.3° at the radial blade elements RP-10 and RP-30. At the stall point, the D-factor at the RP-10 station was very high, 0.75.

At radial measuring stations RP-10, 30, and 50 the deviation angle increased as the rotor approached stall. However, the deviation angle was essentially unaffected by the incidence angle at RP-70, and the deviation angle decreased with increasing incidence angle at RP-90.

The measured values of deviation angle at design flow conditions agree very well

with the design values shown in table II except in the tip region of the blade where the deviation angle was much greater than design.

Stall Performance

The complete noncavitating performance curve of the rotor, including the stall region, is shown in figure 9 where rotor head-rise coefficient for three blade elements is plotted as a function of average flow coefficient. The open symbols are data recorded on an automatic voltage digitizer and computed using a digital computer; the solid symbols were data recorded on a X-Y plotter. Use of the X-Y plotter greatly reduces the amount of operating time in the stall region thereby reducing the chance of possible pump damage in this mode of operation. As flow was reduced from the maximum the head-rise coefficient increased to a peak value (point A) at a flow coefficient of 0.33. Any further throttling beyond point A forced the pump into a stalled condition at a flow coefficient value of 0.32 (point B). Pump operation between points A and B was not possible. Opening the throttle valve moved the pump operating point from point B to point C. Data were not recorded between these two points; operation in this condition was limited because of possible damage to the pump. Further opening of the throttle valve position at point C brought the pump out of stall and returned it to its stable noncavitating flow condition (point D).

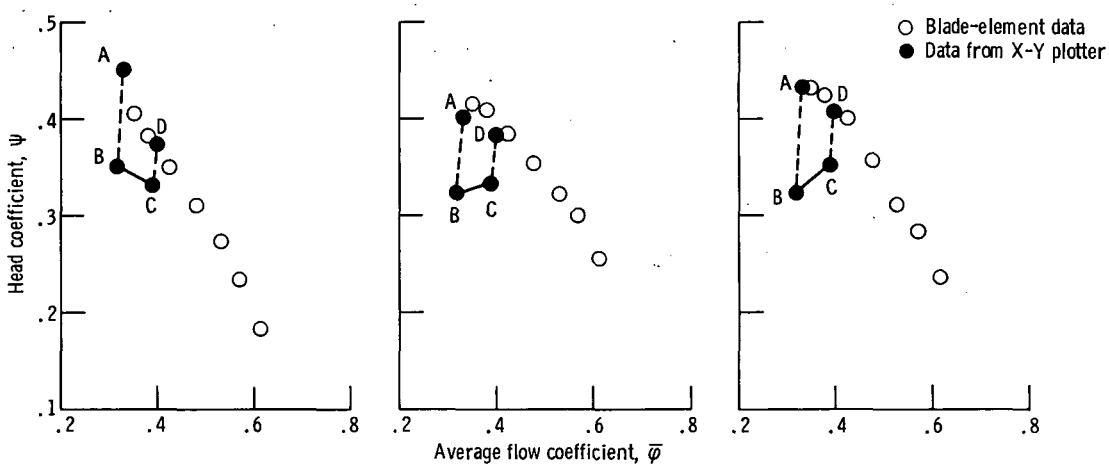

(a) Blade element located at 10 percent of passage height from tip. Radius ratio, 0.98.

(b) Blade element located at 50 percent of passage height from tip. Radius ratio, 0.90.

(c) Blade element located at 90 percent of passage height from tip. Radius ratio, 0.82.

Figure 9. - Rotor blade-element performance (noncavitating). Rotor tip speed, 36 meters per second (118 ft/sec); net positive suction head, 127 meters (415 ft).

SUMMARY OF RESULTS

A 22.9-centimeter (9-in.) diameter axial-flow rotor with a 0.8 hub-tip radius ratio, a design flow coefficient of 0.466, and a blade-tip design diffusion factor of 0.55 was tested. The tests were conducted in 300 K (80^{0} F) water under both cavitating and noncavitating flow conditions. Detailed radial surveys of the flow conditions at the blade inlet and outlet were made, and flow performance parameters were calculated across a number of selected blade elements. The stall hysteresis was recorded at three blade-element locations, and definitions of the outer casing boundary layer were made at the blade inlet and outlet measuring stations. From the tests, the following principal results were obtained:

1. At the rotor tip the outlet flow coefficient was lower and deviation angles were higher than design values. These variations are probably the result of three-dimensional flow effects.

2. At the design flow coefficient, the rotor had an overall head-rise coefficient of 0.360 as compared with the design value of 0.365. An overall hydraulic efficiency of 95.0 percent was measured, which compares favorably with the design value of 92.9 percent.

3. The efficiency remained high (greater than 88 percent) over the entire flow coefficient range which varied from 0.350 to 0.615.

4. From the outer-wall boundary-layer measurements a flow blockage value of 1.29 percent was computed at the blade inlet and remained essentially constant over the whole flow coefficient range of the rotor. Flow blockage values at the blade outlet were computed at 2.69 and 1.40 percent at flow coefficient values of 0.38 and 0.62, respectively.

Lewis Research Center,
National Aeronautics and Space Administration,
Cleveland, Ohio, October 20, 1971,
764-74.

APPENDIX A

SYMBOLS

A	annulus area, m (ft)
C	blade chord, cm (in.)
D	blade diffusion factor, eq. (B8)
g_c	standard acceleration of gravity, 9.8 m/sec^2 (32.174 (lbm)(ft)/(lbf)(sec^2))
H	total head, m (ft)
h_v	vapor pressure head, m (ft)
ΔH	blade element head rise, m (ft)
$\overline{\Delta H}$	mass averaged head rise, m (ft)
i	incidence angle, eq. (B9), deg
NPSH	net positive suction head, eq. (B18), m (ft)
Q_v	venturi measured flow rate, m^3/min (gal/min)
RP	radial position
r	radius, m (ft)
T	thickness, m (ft)
V	velocity, m/sec (ft/sec)
β	flow angle, deg
$\Delta\beta'$	turning angle, deg
γ	blade setting angle
δ	deviation angle, deg, boundary layer thickness (used as a limit of integration in eqs. (B19) and (B20))
δ^*	displacement thickness, eq. (B19), cm (in.)
η	hydraulic efficiency, eq. (B5)
$\overline{\eta}$	mass averaged hydraulic efficiency, eq. (B15)
θ	momentum thickness, eq. (B20), cm (in.)
κ	blade angle, deg
σ	blade solidity
φ	flow coefficient, eq. (B6)
φ^o	blade camber angle, deg
$\overline{\varphi}$	average flow coefficient, eq. (B17)
ψ	head-rise coefficient, eq. (B2)
$\overline{\psi}$	mass averaged head-rise coefficient, eq. (B13)
$\overline{\omega}$	rotor relative total head-loss coefficient, eq. (B7)

Subscripts:

b	blocked
des	design
fs	free stream
h	hub
IW	inner wall
id	ideal
j	index number
max	maximum
OW	outer wall
T	total
t	tip
v	measured with venturi flowmeter
z	axial component

APPENDIX B

EQUATIONS

The equations used to calculate the blade-element and overall performance parameters are now given.

Blade Element Equations

Blade element head rise:

$$\Delta H = H_2 - H_1 \tag{B1}$$

Rotor head-rise coefficient:

$$\psi = \frac{g\,\Delta H}{U_t^2} \tag{B2}$$

Ideal head rise:

$$\Delta H_{id} = \frac{U_2 V_{\theta,2} - U_1 V_{\theta,1}}{g} \tag{B3}$$

Ideal head-rise coefficient:

$$\psi_{id} = \frac{g\,\Delta H_{id}}{U_t^2} \tag{B4}$$

Hydraulic efficiency:

$$\eta = \frac{\Delta H}{\Delta H_{id}}\,100 \tag{B5}$$

Flow coefficient:

$$\varphi = \frac{V_z}{U_t} \tag{B6}$$

Rotor relative total head-loss coefficient:

$$\overline{\omega} = \frac{H'_{2,id} - H'_2}{\frac{V'^2_1}{2g}} = \frac{\Delta H_{id} - \Delta H}{\frac{V'^2_1}{2g}} \tag{B7}$$

Blade diffusion factor:

$$\left.\begin{aligned} D &= 1 - \frac{V'_2}{V'_1} + \frac{r_2 V_{\theta,2} - r_1 V_{\theta,1}}{\sigma V'_1 (r_1 + r_2)} \\ \text{or, for } r_1 = r_2 \qquad D &= 1 - \frac{V'_2}{V'_1} + \frac{\Delta V_\theta}{2\sigma V'_1} \end{aligned}\right\} \tag{B8}$$

Incidence angle:

$$i = \beta'_1 - \kappa_1 \tag{B9}$$

Deviation angle:

$$\delta = \beta'_2 - \kappa_2 \tag{B10}$$

Turning angle:

$$\Delta\beta' = \beta'_1 - \beta'_2 \tag{B11}$$

Overall and Averaged Parameter Equations

Mass averaged head rise:

$$\overline{\Delta H} = \frac{\sum_{j=1}^{j=4} (r_j V_{z,2,j}\, \Delta H_j + r_{j+1} V_{z,2,j+1}\, \Delta H_{j+1})(r_j - r_{j+1})}{\sum_{j=1}^{j=4} (r_j V_{z,2,j} + r_{j+1} V_{z,2,j+1})(r_j - r_{j+1})} \tag{B12}$$

Mass averaged head-rise coefficient:

$$\overline{\psi} = \frac{g\,\overline{\Delta H}}{U_t^2} \tag{B13}$$

Mass averaged ideal head rise:

$$\overline{\Delta H_{id}} = \frac{1}{g}\overline{U_2 V_{\theta,2}} - \overline{U_1 V_{\theta,1}} = \frac{1}{g}\left(\frac{\sum_{j=1}^{j=4} U_{2,j} V_{\theta,2,j} A_{2,j} V_{z,2,j}}{\sum_{j=1}^{j=4} A_{2,j} V_{z,2,j}}\right) - \left(\frac{\sum_{j=1}^{j=4} U_{1,j} V_{\theta,1,j} A_{1,j} V_{z,1,j}}{\sum_{j=1}^{j=4} A_{1,j} V_{z,1,j}}\right) \tag{B14(a)}$$

In this investigation $V_{\theta,1}$ was considered zero in all calculations, so the equation becomes

$$\overline{\Delta H_{id}} = \frac{1}{g}\left(\frac{\sum_{j=1}^{j=4} U_{2,j} V_{\theta,2,j} A_{2,j} V_{z,2,j}}{\sum_{j=1}^{j=4} A_{2,j} V_{z,2,j}}\right) = \frac{\overline{U_2 V_{\theta,2}}}{g} \tag{B14(b)}$$

Mass averaged efficiency:

$$\overline{\eta} = \frac{\overline{\Delta H}}{\overline{\Delta H_{id}}} 100 \tag{B15}$$

Average inlet axial velocity:

$$\overline{V_{z,1}} = \frac{Q_v}{k\pi\left(r_{t,1}^2 - r_{h,1}^2\right)} \tag{B16}$$

where k = 60 meters per second (448.8 ft/sec).
Average inlet flow coefficient:

$$\overline{\varphi} = \frac{\overline{V_{z,1}}}{U_t} \tag{B17}$$

Net positive suction head:

$$NPSH = \overline{H_1} - h_v \tag{B18}$$

Boundary-layer parameter equations:

$$\delta^* = \int_0^{\delta} \left(1 - \frac{V_z}{V_{z,fs}}\right) dy \tag{B19}$$

and

$$\theta = \int_0^{\delta} \frac{V_z}{V_{z,fs}} \left(1 - \frac{V_z}{V_{z,fs}}\right) dy \tag{B20}$$

where δ is the limit of integration in centimeters (or inches).

APPENDIX C

OUTER-WALL BOUNDARY-LAYER MEASUREMENTS

Surveys of flow conditions across the outer-wall boundary layer at noncavitating conditions were made at the rotor inlet and outlet measuring stations for a range of flows. The measurements were used primarily to obtain flow blockage values.

The velocity profiles at the rotor inlet measuring station are shown in figure 10. Velocity ratios are presented as the ratio of local velocity to free-stream velocity. The velocities are computed from boundary-layer surveys of total pressure, flow angle, and outer-wall static-pressure measurements. The boundary-layer parameters (displacement thickness δ^* and momentum thickness θ) were computed from the velocity profiles shown. At the inlet measuring station flow angle measurements indicated that the flow direction was essentially axial; therefore, the boundary layer was considered to be two dimensional. Boundary-layer measurements were made out to the RP-10 measuring station (0.229 cm (0.090 in.) from the outer wall). The velocity distribution showed that

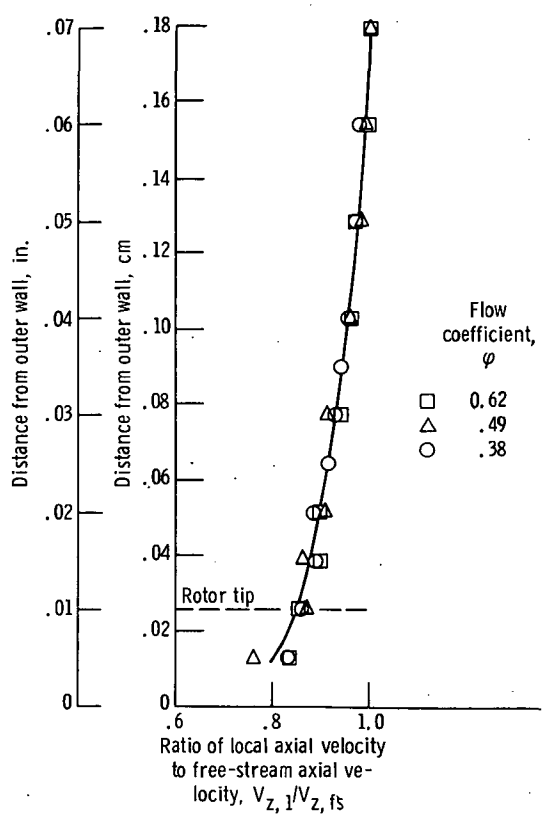

Figure 10. - Velocity distribution across outer-wall boundary layer at rotor inlet. Displacement thickness, 0.0147 centimeter (0.0058 in.); momentum thickness, 0.01270 centimeter (0.0050 in.).

a constant free-stream velocity was maintained to approximately 0.178 centimeter (0.070 in.) from the outer wall. Free-stream velocity was defined as the value measured at the RP-10 radial location. The velocity ratio distribution was essentially the same over the whole flow range of the rotor. The boundary-layer thickness was set at 0.070 inch (0.178 cm) in all flow-parameter calculations at the inlet. The computed values of δ^* and θ were 0.0147 and 0.0127 centimeter (0.0058 and 0.0050 in.), respectively. The same value of displacement thickness was assumed for the hub shroud. Area blockage factors were computed for both inner and outer walls and are presented in table III as the ratio of the blocked area A_b to the total annulus area A in percent.

TABLE III. - BOUNDARY-LAYER BLOCKAGE AT ROTOR INLET AND OUTLET

Flow coefficient, φ	Ratio of blocked area to total annulus area, percent		
	Outer wall, $(A_b/A)_{OW}$	Inner wall, $(A_b/A)_{IW}$	Total $(A_b/A)_T$
Rotor inlet			
0.62 and 0.38	0.72	0.57	1.29
Rotor outlet			
0.62 .38	0.78 1.49	0.62 1.20	1.40 2.69

With the flow blockage of 1.29 percent, the design inlet flow diagrams should be achieved at a measured average flow coefficient of

$$\overline{\varphi} = (1 - 0.0129)\,\overline{\varphi}_{des}$$

$$\overline{\varphi} = (0.9871)(0.466) = 0.460$$

At the rotor outlet measuring station the boundary-layer flow has both axial and tangential velocity components. This skewed boundary-layer flow is further complicated by the 0.025-centimeter (0.010-in.) tip clearance between the housing and the rotating blade. For these reasons calculation of boundary-layer parameters at this axial station was limited to a displacement thickness based on the through-flow velocity component $V_{z,2}$. The axial and tangential components of the boundary-layer velocities are presented in figure 11. As shown by the outlet axial velocity distribution, the boundary-

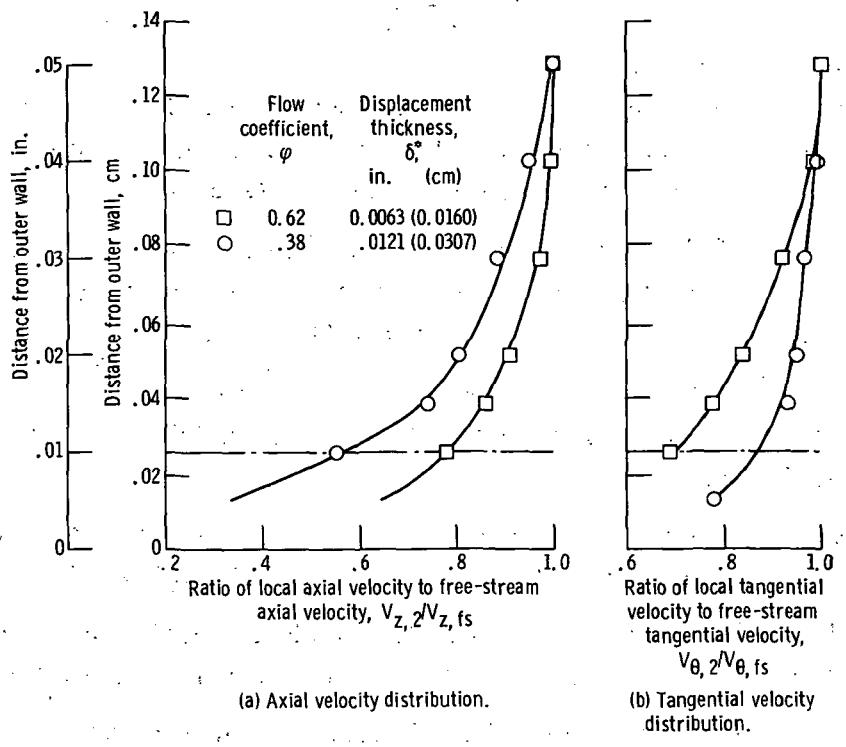

(a) Axial velocity distribution.

(b) Tangential velocity distribution.

Figure 11. - Velocity distribution across outer-wall boundary layer at rotor outlet.

layer thickness δ varied with the flow range. Free-stream velocities were maintained to radial locations of approximately 0.127 and 0.076 centimeter (0.050 and 0.030 in.) from the outer wall for flow coefficient values of 0.38 and 0.62, respectively. These values were used for the physical boundary-layer thicknesses in the displacement thickness calculations. Computed values of δ^* were 0.0307 and 0.0160 centimeter (0.0121 and 0.0063 in.) for the flow-coefficient values of 0.38 and 0.62, respectively. Using these same values of δ^* for the hub shroud, area blockages were computed for both the inner and outer walls at the outlet measuring for both flow coefficient values, and the results are shown in table III.

REFERENCES

1. Lieblein, Seymour; Schwenk, Francis C.; and Broderick, Robert L.: Diffusion Factor for Estimating Losses and Limiting Blade Loadings in Axial-Flow-Compressor Blade Elements. NACA RM E53D01, 1953.

2. Crouse, James E.; Soltis, Richard F.; and Montgomery, John C.: Investigation of the Performance of an Axial-Flow-Pump Stage Designed by the Blade-Element Theory - Blade Element Data. NASA TN D-1109, 1961.

3. Crouse, James E.; and Sandercock, Donald M.: Blade-Element Performance of 0.7 Hub-Tip Radius Ratio Axial-Flow-Pump Rotor with Tip Diffusion Factor of 0.43. NASA TN D-2481, 1964.

4. Urasek, Donald C.: Design and Performance of a 0.9-Hub-Tip-Ratio Axial-Flow Pump Rotor with a Blade-Tip Diffusion Factor of 0.63. NASA TM X-2235, 1971.

5. Miller, Max J.; and Sandercock, Donald M.: Blade Element Performance of Axial-Flow Pump Rotor with Blade Tip Diffusion Factor of 0.66. NASA TN D-3602, 1966.

6. Miller, Max J.; and Crouse, James E.: Design and Overall Performance of an Axial-Flow Pump Rotor with a Blade-Tip Diffusion Factor of 0.66. NASA TN D-3024, 1965.

NASA-Langley, 1971 — 1 E-6423

NATIONAL AERONAUTICS AND SPACE ADMISTRATION
WASHINGTON, D.C. 20546

OFFICIAL BUSINESS
PENALTY FOR PRIVATE USE $300

FIRST CLASS MAIL

POSTAGE AND FEES PAID
NATIONAL AERONAUTICS AND
SPACE ADMINISTRATION

U.S.MAIL

POSTMASTER: If Undeliverable (Section 158 Postal Manual) Do Not Return

"The aeronautical and space activities of the United States shall be conducted so as to contribute . . . to the expansion of human knowledge of phenomena in the atmosphere and space. The Administration shall provide for the widest practicable and appropriate dissemination of information concerning its activities and the results thereof."

—NATIONAL AERONAUTICS AND SPACE ACT OF 1958

NASA SCIENTIFIC AND TECHNICAL PUBLICATIONS

TECHNICAL REPORTS: Scientific and technical information considered important, complete, and a lasting contribution to existing knowledge.

TECHNICAL NOTES: Information less broad in scope but nevertheless of importance as a contribution to existing knowledge.

TECHNICAL MEMORANDUMS: Information receiving limited distribution because of preliminary data, security classification, or other reasons.

CONTRACTOR REPORTS: Scientific and technical information generated under a NASA contract or grant and considered an important contribution to existing knowledge.

TECHNICAL TRANSLATIONS: Information published in a foreign language considered to merit NASA distribution in English.

SPECIAL PUBLICATIONS: Information derived from or of value to NASA activities. Publications include conference proceedings, monographs, data compilations, handbooks, sourcebooks, and special bibliographies.

TECHNOLOGY UTILIZATION PUBLICATIONS: Information on technology used by NASA that may be of particular interest in commercial and other non-aerospace applications. Publications include Tech Briefs, Technology Utilization Reports and Technology Surveys.

Details on the availability of these publications may be obtained from:

SCIENTIFIC AND TECHNICAL INFORMATION OFFICE

NATIONAL AERONAUTICS AND SPACE ADMINISTRATION

Washington, D.C. 20546